Space Weather

RESEARCH ARTICLE
10.1029/2019SW002347

Special Section:
Outcomes of the Applied Space Environments Conference, May 12-17, 2019, Los Angeles, CA

Correcting the Arcjet Thruster Disturbance in GOES-16 Magnetometer Data

S. Califf[1], D. Early[2], M. Grotenhuis[3], T. M. Loto'aniu[1], and J. Kronenwetter[2]

[1]Cooperative Institute for Research in Environmental Sciences, NOAA National Centers for Environmental Information, Boulder, CO, USA, [2]Chesapeake Aerospace, NASA Goddard Space Flight Center, Greenbelt, MD, USA, [3]Science Systems and Applications, Inc., NASA Goddard Space Flight Center, Greenbelt, MD, USA

Abstract The GOES-R series magnetometers provide observations of the Earth's magnetic field at geostationary orbit for operational use by National Oceanic and Atmospheric Administration (NOAA)'s Space Weather Prediction Center. The GOES-R spacecraft use arcjet thrusters for orbital stationkeeping, and the partially ionized thruster plume creates a relatively large (~20 nT) disturbance in the magnetometer data. This study presents a correction algorithm that removes the arcjet signal from the magnetometer data. The algorithm is based on an observed linear relationship between the arcjet disturbance and the ambient magnetic field. We estimate correction parameters using data from GOES-16 (the first spacecraft of the GOES-R series), evaluate the uncertainties in the corrected data during arcjet events, and discuss limitations and considerations for arcjet correction in the GOES-R series magnetometers.

Key Points:
- Arcjet thrusters create a ~20 nT disturbance in the GOES-16 magnetometer data that is linearly related to the ambient magnetic field
- A correction algorithm is presented that removes the effect of the arcjets in the magnetometer data
- Uncertainties and limitations of the arcjet correction are discussed

Correspondence to:
S. Califf,
califf@colorado.edu

Citation:
Califf, S., Early, D., Grotenhuis, M., Loto'aniu, T. M., & Kronenwetter, J. (2020). Correcting the arcjet thruster disturbance in GOES-16 magnetometer data. *Space Weather*, *18*, e2019SW002347. https://doi.org/10.1029/2019SW002347

Received 30 AUG 2019
Accepted 4 JAN 2020
Accepted article online 10 JAN 2020

1. Introduction

GOES magnetometers have been continuously monitoring the geomagnetic field at geostationary orbit for over 40 years. The data are used at National Oceanic and Atmospheric Administration (NOAA)'s Space Weather Prediction Center for space weather situational awareness, such as detecting geomagnetic storms, substorms, and movement of the magnetopause inside geostationary orbit (e.g., Sibeck et al., 2000; Singer et al., 1996). Local magnetic field measurements are required to provide pitch angle information for the energetic particle detectors onboard GOES (Dichter et al., 2015). The magnetometer data are also used to validate emerging operational space weather models, and it is expected that high-resolution GOES magnetometer data will be an important input to future radiation belt models for knowledge of the local magnetic field, the global magnetospheric configuration, and ultralow-frequency waves that affect radial diffusion and loss of radiation belt electrons (e.g., Shprits et al., 2008; Shprits et al., 2008). In addition to the primary operational purpose, GOES magnetometer data have also been used extensively in scientific research (e.g., Iijima et al., 1993; Nagai et al., 2019; Singer et al., 1983; Takahashi et al., 2011; Tsyganenko & Sitnov, 2005), which plays an important role in developing operational space weather capabilities. Given the wide-ranging applications of GOES magnetometer data, it is critical to understand measurement errors, flag erroneous data for end users, and correct the data when possible.

The GOES-R spacecraft use hydrazine arcjet thrusters for periodic orbital maneuvers to maintain the desired geostationary location. During arcjet operation, the magnetometer measurements are corrupted by ~20 nT, which is significant relative to the typical 100 nT geomagnetic field magnitude at geostationary orbit. Arcjet thrusters apply an electrical current to the propellant at the thruster nozzle, heating the exhaust and increasing thrust and efficiency (e.g., Bogorad et al., 2008). Although only a small fraction (~1%) of the thruster plume is ionized, the density of the ionized portion of the plume is much higher than the typical ambient density in the geostationary environment. The thruster plume plasma density is sufficient to alter the magnetic field near the spacecraft, and the observations indicate a diamagnetic reduction in the ambient field primarily along the thrust axis and offsets independent of the ambient field that vary with the relative location of the magnetometer and the arcjet thruster. Detailed discussion of the structure of the arcjet disturbance and potential physical mechanisms inferred from measurements by the inboard (IB) and outboard (OB) magnetometers can be found in Califf et al. (2019).

This study expands on the observations of arcjet thruster contamination on the GOES-16 magnetometer and physical interpretation presented in Califf et al. (2019) to derive a correction to the GOES-16 magnetometer data during arcjet events. This paper presents the method for correcting the arcjet disturbance using

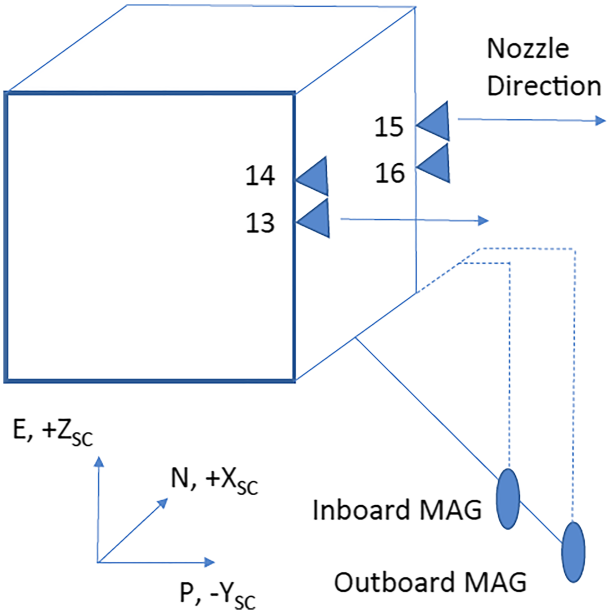

Figure 1. Schematic of the GOES-16 magnetometers and arcjet thrusters [adapted from Califf et al., 2019]. The axes show the relationship between earthward-poleward-normal and spacecraft-fixed coordinates (*XYZ*) when the spacecraft is in the nominal nadir-pointing attitude mode.

GOES-16 as an example. The final operational algorithm will include unique correction parameters derived for each spacecraft in the GOES-R series. The GOES-16 magnetometers, arcjet thrusters, and data used in this study are described in section 2. Characteristics of the magnetic disturbance produced by the arcjets and correlation with the ambient magnetic field are presented in section 3, and a correction for the arcjet contamination is derived and applied to the data in section 4. The uncertainties in the corrected data are discussed in section 5, and section 6 summarizes the results.

2. GOES-16 Spacecraft Diagram and Magnetometer Data

2.1. GOES-16 Magnetometer and Arcjet Thruster Configuration

The relative locations of the magnetometers and the arcjet thrusters on GOES-16 are displayed in Figure 1. GOES-16 has two triaxial fluxgate magnetometers mounted on an 8.5 m boom, with the OB magnetometer located at the end of the boom and the IB magnetometer along the boom 6.3 m from the spacecraft. Magnetic field vectors are sampled at 10 Hz with an effective frequency response of 2.5 Hz due to an antialiasing filter. For more details on the GOES-R magnetometers, see Loto'aniu et al. (2019).

There are four arcjet thrusters pointing in the $-Y$ direction in the spacecraft frame. The magnetometer boom extends away from the spacecraft bus in the $-Z$ direction and is canted toward $+X/-Y$. Stationkeeping maneuvers typically occur every 4 days and last ~90 min, and each maneuver uses two of the arcjet thrusters in either even (thrusters 14/16) or odd (thrusters 13/15) pairs.

2.2. Data

This study uses publicly available level 2 GOES-16 magnetometer data from the National Centers for Environmental Information (NCEI), which can be found at https://data.ngdc.noaa.gov/platforms/solar-space-observing-satellites/goes/goes16/l2/data/magn-l2-hires/. Level 1b data are the raw data from the spacecraft converted to physical units using initial ground-based correction parameters for temperature compensation, alignment, and scale factor. Level 1b data are produced by the GOES-R ground segment and are uplinked and rebroadcast from the spacecraft in real time. NCEI reprocesses level 1b data to produce level 2 data, which includes 10 Hz and 1-min averaged vector magnetic field measurements expressed in various coordinate systems. This study analyzes arcjet magnetic signatures and corrections in the earthward-poleward-normal (EPN) coordinate system (e.g., Loto'aniu et al., 2019), which is roughly aligned with the Earth's magnetic field in the *P* component and is effectively fixed with respect to the spacecraft during nominal nadir-pointing operations (see Figure 1). The arcjet flag indicating times when the arcjets are firing has been available in the level 2 data since 18 October 2018, and the corrections for the arcjet disturbance described in this paper have recently been implemented in the NOAA level 1b data.

3. Arcjet Signature in the Magnetometer Data and Correlation With the Ambient Magnetic Field

3.1. Arcjet Magnetic Disturbance

An example of the arcjet signature in the GOES-16 magnetometer data is plotted in Figure 2. The primary disturbance is in the *P* (poleward) component of the magnetic field, which is aligned with the thrust axis when GOES-16 is in the nominal operational attitude configuration. The *P* component is also generally aligned with the geomagnetic field at geostationary orbit, although the field direction can vary significantly (>45 deg) depending on local time and geomagnetic activity. The disturbance appears as a step-like reduction in the magnetic field of ~20 nT, which is 20% of the typical 100 nT magnetic field strength at geostationary orbit.

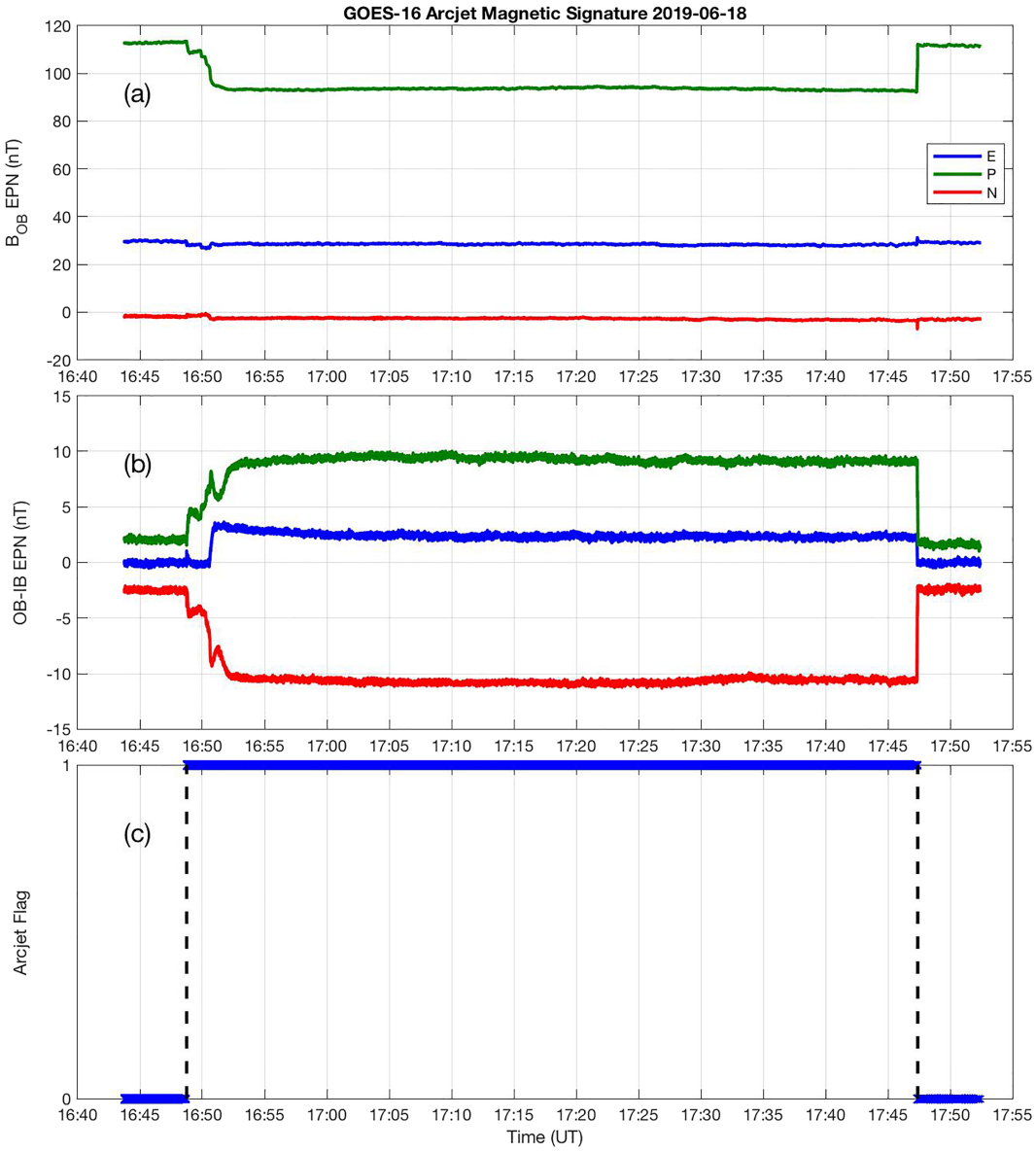

Figure 2. Example arcjet signature for GOES-16 on 18 June 2019. (a) Measured magnetic field from the outboard magnetometer in earthward-poleward-normal coordinates, (b) difference between the outboard and inboard magnetometers, and (c) arcjet flag indicating times when the thrusters are firing.

Differences between the OB and IB magnetometers (Figure 2b) indicate that after an initial transient at the beginning of the burn, the error introduced by the arcjet thrusters is relatively stable and that the disturbance rapidly decays when the thrusters are turned off. Small differences between the OB and IB magnetometers before and after the arcjet burn are primarily due to known diurnal bias variations on GOES-16 (Loto'aniu et al., 2019), although some small residual bias errors (~1–2 nT) related to the arcjets have been identified that can last 2–3 hr after the end of the arcjet event.

3.2. Estimating the Magnitude of the Arcjet Disturbance

The rapid recovery after the arcjets are turned off is shown in detail in Figure 3. There are four arcjet thrusters, and each arcjet event uses either the even (thrusters 14/16) or odd (thrusters 13/15) pair. The two-step response in Figure 3 corresponds to the thrusters being turned off sequentially.

The response in Figure 3 is faster than typical variations in the geomagnetic field during quiet times, so differences in the measurement immediately before and after the arcjets are turned off primary reflect the

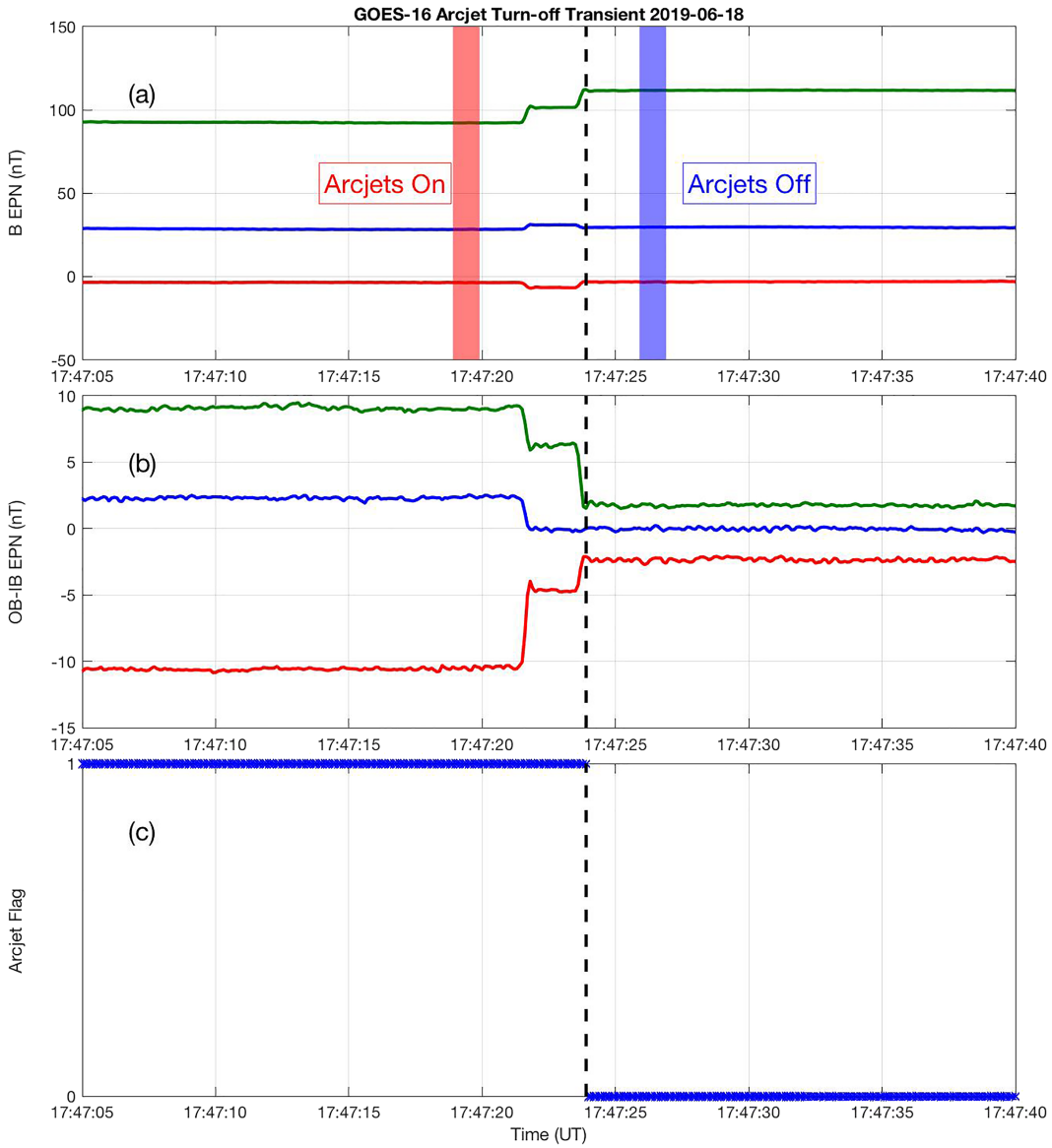

Figure 3. Example transient at the end of the arcjet burn on 4 July 2019. (a) Outboard magnetometer measurements, with red and blue shaded areas indicating the averaging periods for determining the change in the measurement when the arcjets are turned off; (b) difference between the outboard and inboard magnetometers; and (c) arcjet flag.

magnetic deviation introduced by the arcjets for each event. Fast geomagnetic variations with second timescales, such as electromagnetic ion cyclotron waves (~1–2 Hz; e.g., Engebretson et al., 2015), are present in the GOES data and could increase uncertainty in the analysis. We have not excluded wave events in this paper, but these events can be easily identified and excluded from the dataset for determining the final operational correction parameters. One-second averages were used to compute the "on" and "off" measurements, with the on interval (Figure 3a, red shaded area) beginning 5 s before the arcjet flag indicates that the thrusters have turned off, and the off interval (Figure 3a, blue shaded area) beginning 2 s after the flag returns to zero. The off measurement represents the undisturbed ambient magnetic field, which will be used in the next section to determine a correlation between the arcjet disturbance and the ambient field.

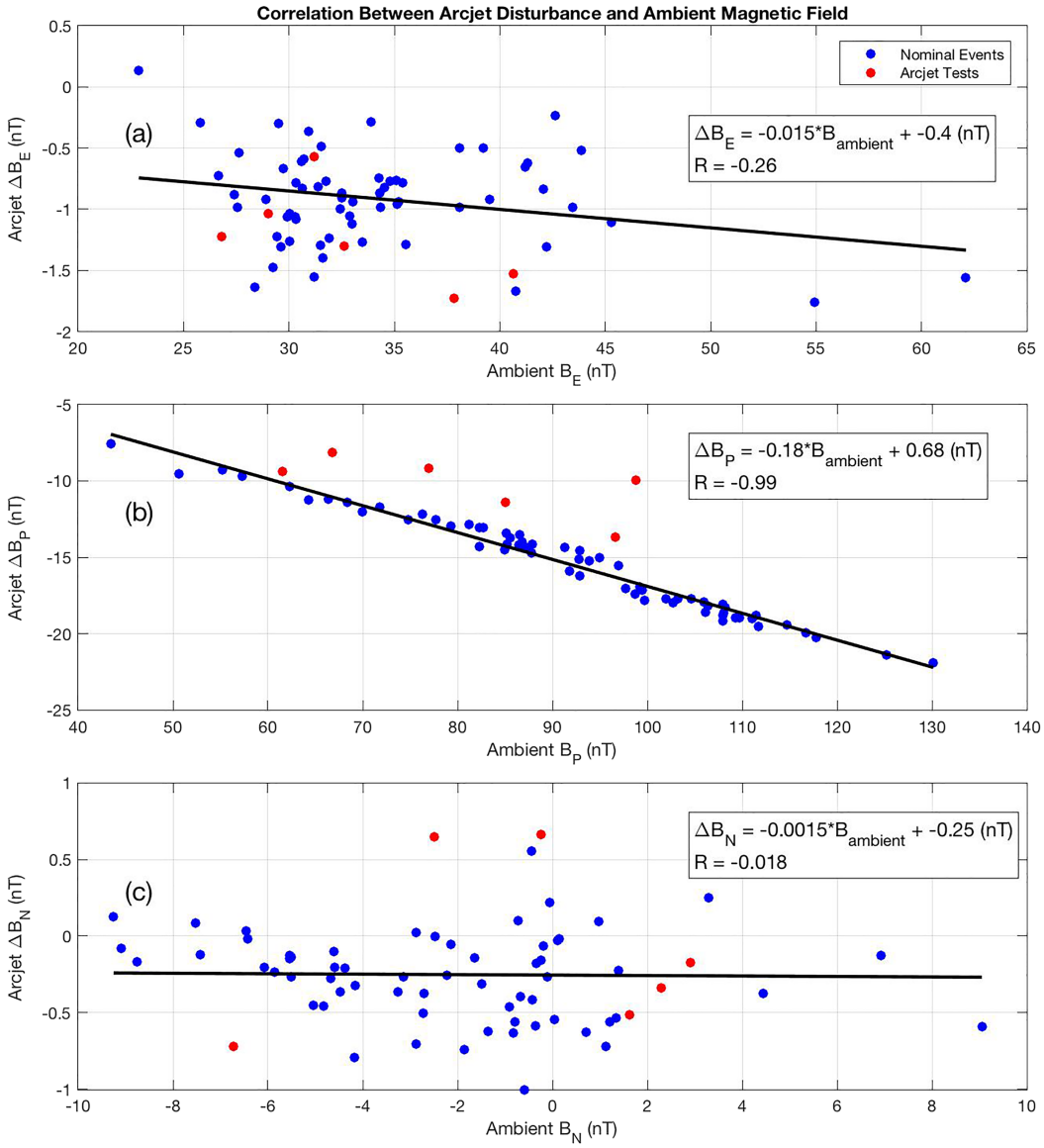

Figure 4. Change in the GOES-16 outboard magnetometer measurement as a function of ambient magnetic field strength in earthward-poleward-normal coordinates. The linear relationship between the arcjet disturbance, ΔB, and the ambient magnetic field, B_{ambient}, is shown for each earthward-poleward-normal component.

3.3. Relationship Between the Arcjet Disturbance and the Ambient Magnetic Field

The arcjet disturbance is plotted against the ambient magnetic field in Figure 4 based on 63 GOES-16 arcjet events between 18 October 2018 and 12 August 2019. The data were derived from the difference in the measurement at the end of each arcjet burn described in section 3.2, and the measurement in the off state was used to estimate the undisturbed ambient magnetic field. Some uncertainty exists in the ambient field estimate due to known bias variations in the magnetometers, including a small (1–2 nT) residual bias error related to electronics heating caused by the arcjet thrusters' electronic power control unit located next to the magnetometer electronics units. Six events have been removed from the dataset because they involved known diagnostic tests on the arcjets (Figure 4, red dots). These events produced out-of-family magnetic signatures between 2 and 7 nT that were apparent in the magnetometer data without knowledge of the arcjet tests.

There is a strong linear correlation ($R = -0.99$) between the P component disturbance and the P component of the ambient magnetic field, and there are smaller offsets in the E and N components that are effectively uncorrelated with the ambient magnetic field. There are weaker cross correlation terms between axes ($R < 0.6$) that are not shown but are included in the correction algorithm.

The P component is aligned with the thrust axis and is also aligned roughly with the main component of the geomagnetic field, although the geomagnetic field direction varies by up to 51 deg from the P axis in this dataset. The correlation along the thrust axis suggests a diamagnetic effect where the plasma in the thruster plume partially cancels the local magnetic field. This interpretation is supported by plume plasma density and temperature estimates and a basic derivation of the expected diamagnetic response (Califf et al., 2019; Likar et al., 2006; Pollard et al., 2001). There is a spatial dependence to the offsets in the E and N components determined by measurements from each thruster at the IB and OB magnetometers that suggests that the offsets are driven by plasma pressure gradients within the expanding thruster plume. More details on the effects of individual arcjet thrusters at both the IB and OB magnetometers can be found in Califf et al. (2019).

4. Arcjet Disturbance Correction

Given the observed linear relationship between the arcjet disturbance and the ambient magnetic field, the following correction is proposed:

$$B_{\text{corrected}} = T_{\text{correction}} B_{\text{measured}} + B_{\text{bias}} \tag{1}$$

where $B_{\text{corrected}}$ is the corrected magnetic field measurement during arcjet operations, $T_{\text{correction}}$ is a 3×3 matrix relating the measured disturbed magnetic field to the ambient field, and B_{bias} is a bias term to account for static offsets when the arcjets are firing. This correction assumes that the linear relationship between the arcjet disturbance and the ambient magnetic field estimated from the turn-off transient is consistent throughout the arcjet burn. The correction is analyzed in EPN coordinates in this study, although the method could be applied using any spacecraft-fixed coordinate system.

The correction parameters for the OB magnetometer are determined through a least squares estimate using the 63 events.

$$T_{\text{correction OB}} = \begin{bmatrix} 1.024 & 0.013 & 0.023 \\ 0.063 & 1.221 & -0.034 \\ -0.013 & 0.014 & 1.037 \end{bmatrix} \tag{2}$$

$$B_{\text{bias OB}} = \begin{bmatrix} -0.79 \\ -3.61 \\ -0.31 \end{bmatrix} (nT) \tag{3}$$

The IB magnetometer correction is less reliable due to known bias stability problems, so the primary focus is to correct the OB magnetometer data. The IB correction terms are provided below for reference.

$$T_{\text{correction IB}} = \begin{bmatrix} 0.995 & 0.077 & 0.092 \\ 0.010 & 1.207 & -0.002 \\ -0.038 & -0.058 & 1.040 \end{bmatrix} \tag{4}$$

$$B_{\text{bias IB}} = \begin{bmatrix} -3.55 \\ 6.16 \\ -1.62 \end{bmatrix} (nT) \tag{5}$$

Figure 5 shows an example of corrected OB magnetometer data (green line) during arcjet operations on 18 June 2019. The correction from equation (1) is applied to data with a positive arcjet flag. The correction removes most of the ~20-nT step response in the P component, and the corrected data closely align with the undisturbed data just before and after the arcjets fire. Geophysical variations and noise levels are also qualitatively consistent before, during, and after the arcjet event, indicating that there are not significant

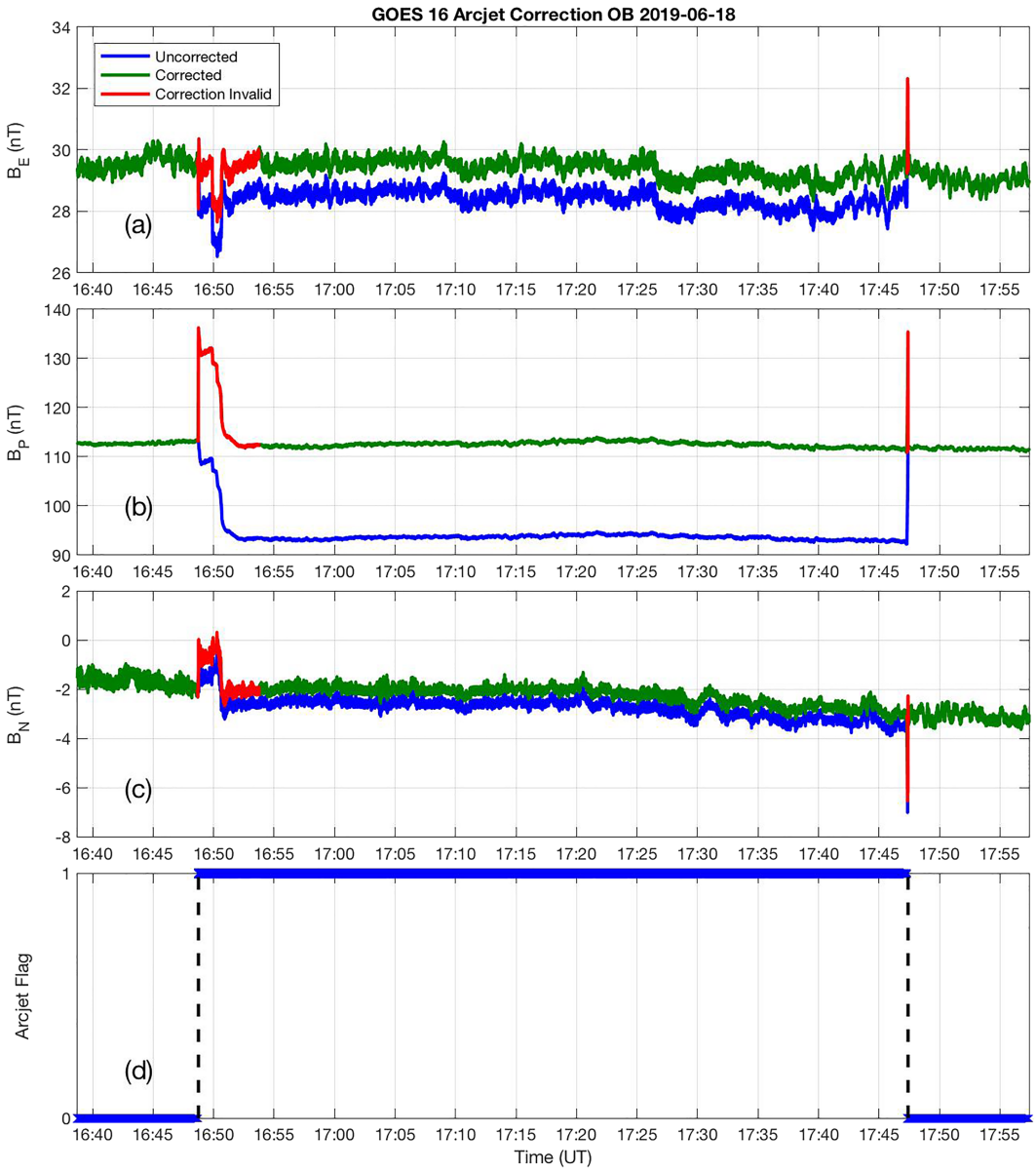

Figure 5. Corrected magnetometer data during an arcjet event on 18 June 2019.

additional time-varying errors related to the arcjets other than the linear relationship with the ambient magnetic field. The algorithm does not account for transients at the beginning and end of the arcjet burn (red line). These transients are indicated by a correction validity flag in the level 1b data.

The difference between the OB and IB magnetometers during the startup transient is plotted in Figure 6. OB-IB differences remove geophysical variations and reveal the relative errors between the two magnetometers. At the beginning of the arcjet burn, the currents to the thrusters are slowly ramped up, and the gradual increase in the magnetic disturbance is not captured by the simple static linear correction of the measured data. The correction is derived at the end of the arcjet burn when the thrusters have reached a steady state condition.

GOES-16 has known bias variations that generally repeat from day to day but vary on seasonal timescales. The OB-IB difference from the previous day (Figure 6, red line) can be used as a metric for determining the validity of the correction, as the corrected data should follow the pattern from the previous day. The settling time of the startup transient varies between axes but converges to the OB-IB

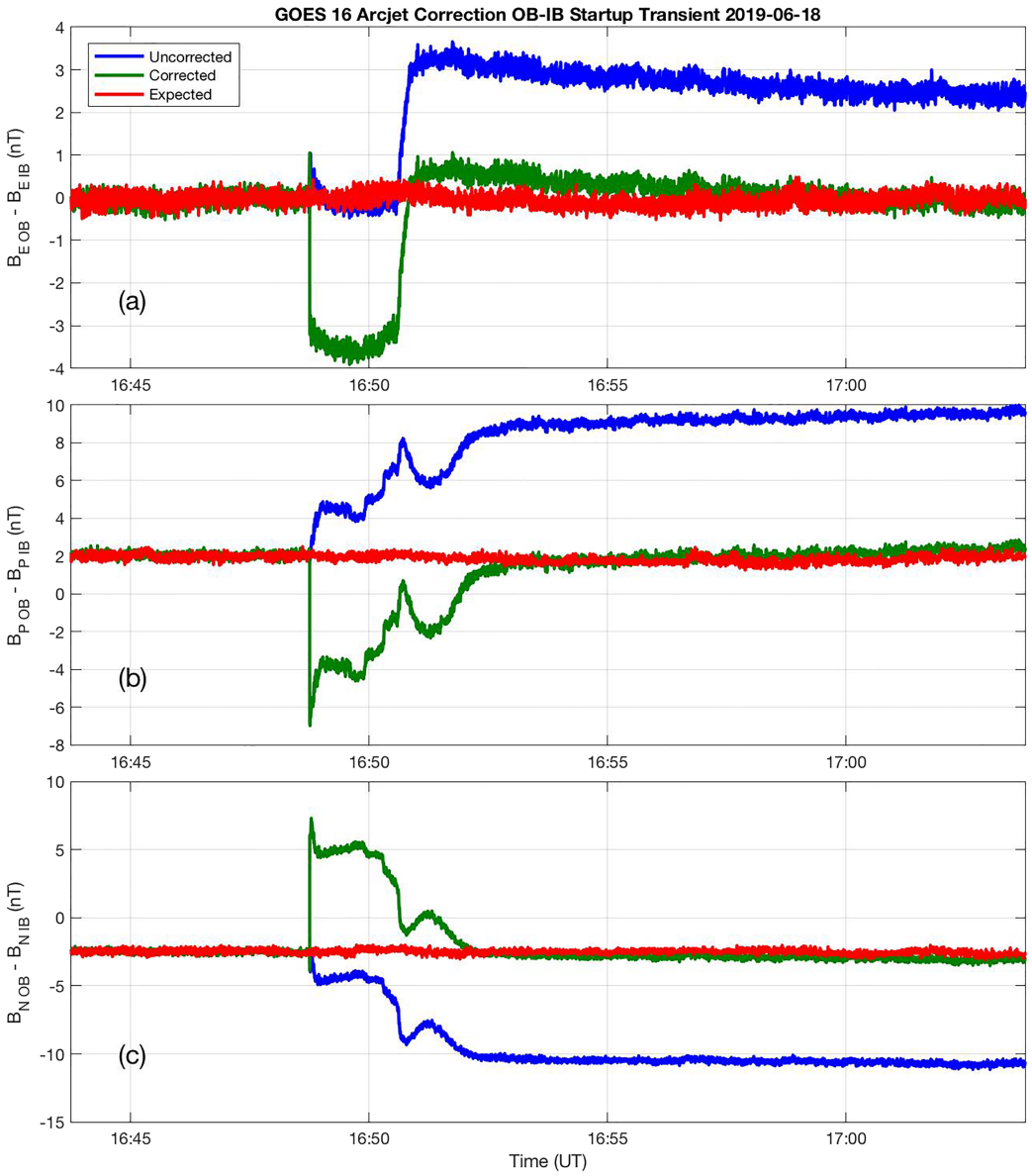

Figure 6. Difference between the outboard and inboard magnetometers during the startup transient on 18 June 2019. The outboard-inboard difference at the same time on the previous day (red line) is the expected difference after correction.

difference from the previous day within 4–5 min of the beginning of the arcjet burn. Based on reviewing all of the startup transients, there are consistent patterns that support a potential startup transient correction in future work. The initial correction algorithm will include an additional flag for validity of the corrected data, and the corrected data during the first 5 min of the arcjet burn will be flagged as invalid.

The corrected data during the turn-off transient are plotted in Figure 7 (green line). There is a rapid step in the corrected data just before the arcjet flag indicates that the thrusters are off. The two steps correspond to the two thrusters being turned off sequentially, and the intermediate states could potentially be corrected because they are repeatable (Califf et al., 2019). Since the data are used in real-time operations, the correction validity flag will be triggered based on the commanded burn duration in order to mark the data as invalid at least 5 s before the arcjets are turned off.

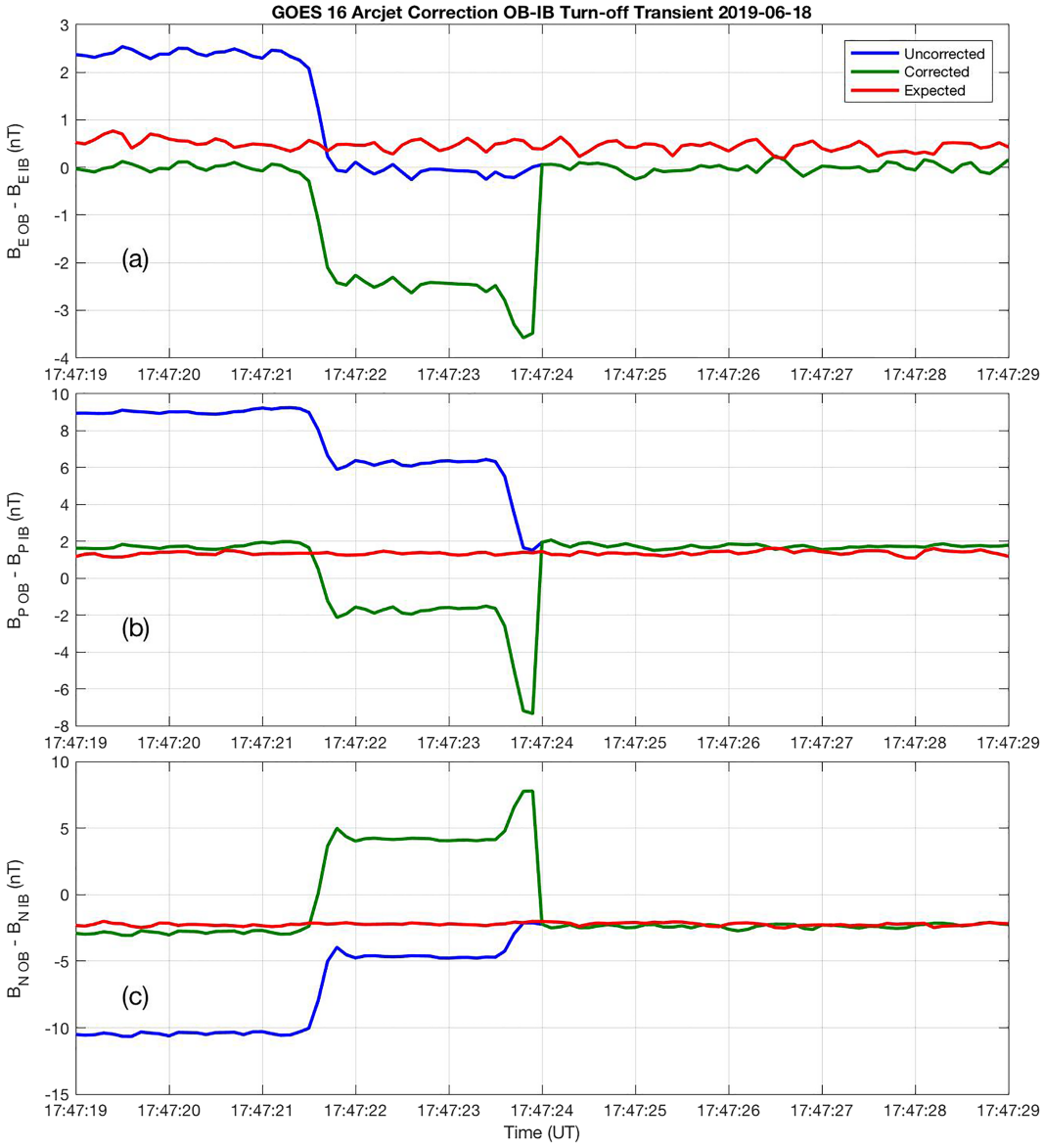

Figure 7. Difference between the outboard and inboard magnetometers during the turn-off transient on 18 June 2019. The outboard-inboard difference at the same time on the previous day (red line) is the expected difference after correction.

5. Arcjet Correction Uncertainty and Limitations

5.1. Correction Residuals

Figure 8 shows the correction residuals calculated by comparing the corrected magnetic field 5 s before the arcjets were turned off to the measured magnetic field 2 s after the end of the burn. The residuals suggest that the arcjet disturbance can be corrected to within 1.5 nT or better. However, there are several factors that may cause the true error to be larger than 1.5 nT. This result assumes that the linear relationship between the arcjet disturbance and the ambient magnetic field is consistent throughout the entire arcjet burn. The startup transient indicates that the relationship is not constant but does settle to a consistent behavior after ~5 min. Also, the residuals are computed from the same dataset used to derive the correction. It is possible that the arcjet performance will vary over time, so the correction should be reevaluated periodically.

The correction parameters are computed over a limited range of ambient magnetic field values and orientations relative to the thruster, and environmental conditions outside of this dataset may not follow the same behavior. The diamagnetic effect depends on the balance of the magnetic and particle pressure inside and

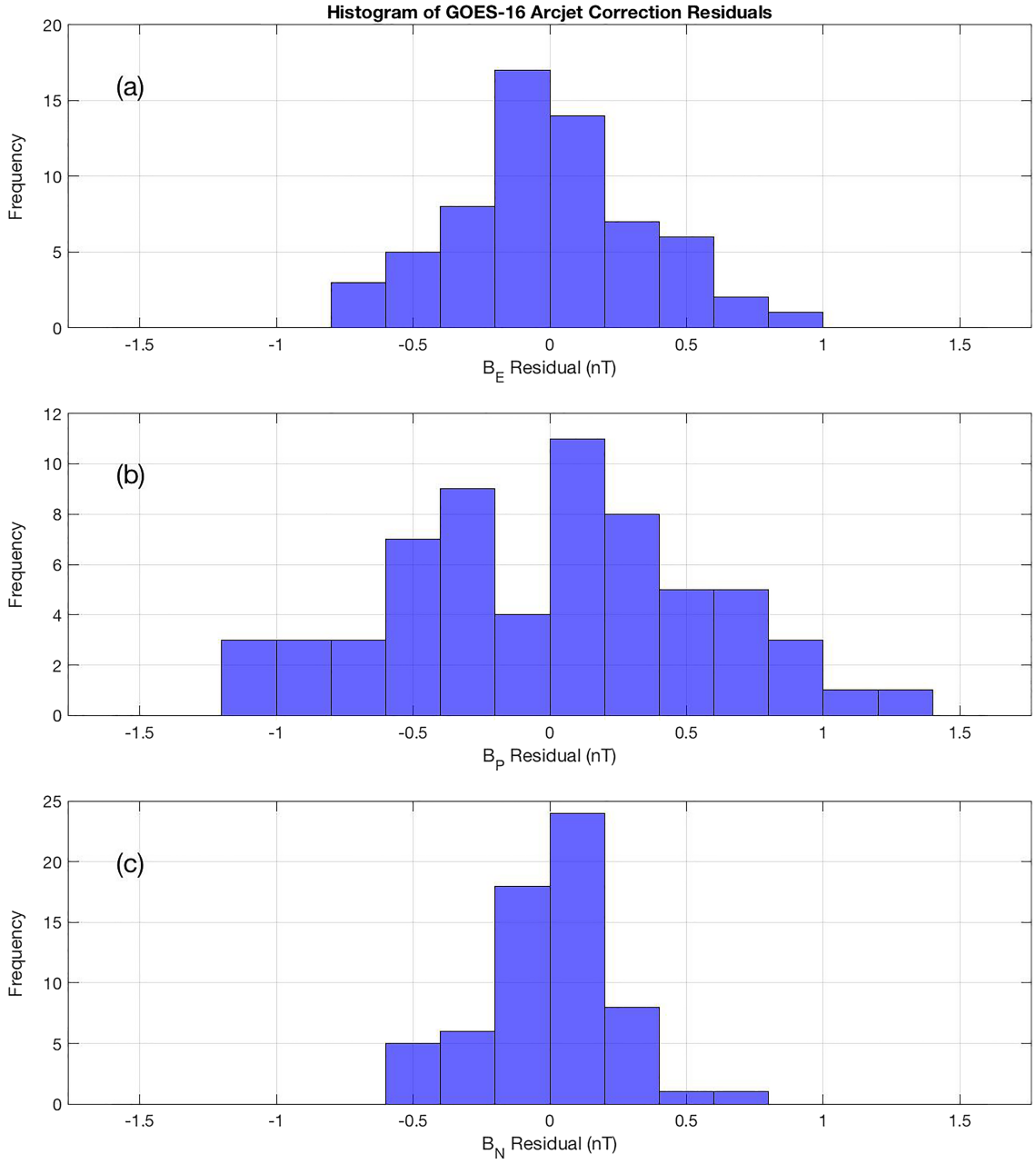

Figure 8. Histogram of correction residuals at the end of each arcjet event.

outside of the thruster plume (Califf et al., 2019), and the assumption is that the ambient magnetic pressure dominates the ambient particle pressure. There may be variations in this relationship if the ambient particle pressure becomes significant relative to the ambient magnetic pressure, such as during substorm injections (e.g., Cohen et al., 2017).

The arcjet correction will need to be recomputed for each GOES-R series spacecraft to account for specific arcjet thruster performance. This study only evaluates magnetic disturbances related to odd pair arcjet thrusters on GOES-16, but each GOES-R spacecraft has two sets of available arcjet thrusters that produce unique magnetic signatures. The correction algorithm currently being implemented in the GOES-R ground processing software applies a correction that is specific to the thruster pair in use. Also, the second GOES-R series satellite, GOES-17, performs semiannual yaw flips, where the spacecraft is inverted about the nadir vector.

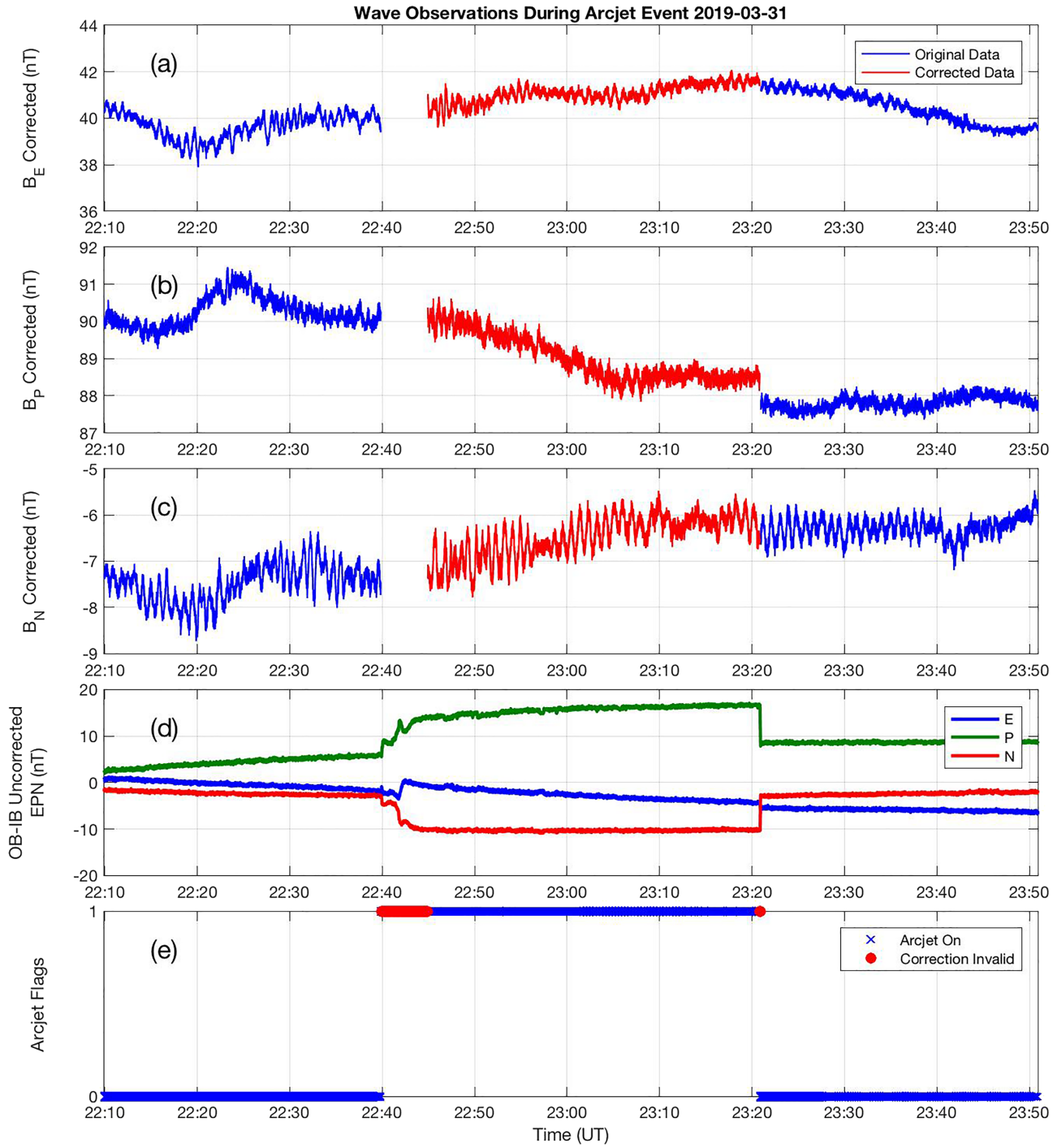

Figure 9. Wave observations during an arcjet event on 31 March 2019. (a–c) Measured magnetic field from the outboard magnetometer, including corrected data during the arcjet burn (red line), (d) uncorrected outboard-inboard difference, (e) arcjet flag, and arcjet correction flag indicating invalid correction times at the beginning and end of the burn.

The yaw flip reverses the direction of the thruster with respect to the nominal geomagnetic field and may alter the relationship between the arcjet disturbance and the ambient magnetic field.

5.2. Wave Observations During Arcjet Operation

An example of a geomagnetic wave event overlapping an arcjet burn is plotted in Figure 9. These are ultralow-frequency waves with an ~1-min period and a peak-to-peak amplitude of ~1 nT. The wave event

starts 30 min before the arcjets turn on and persists until 30 min after the arcjets turn off. The characteristics of the wave observations in the data corrected for arcjet contamination (red line) are qualitatively similar to the uncorrupted data (blue line). This suggests that wave data may be valid for some applications during arcjet operation, although caution should be used when interpreting corrected wave data because the arcjets emit dense plasma that may generate waves or alter the behavior of existing waves. The overall instrument noise level when the arcjets are firing appears to be similar to the baseline noise in the OB time series (Figures 9a–9c) and the OB-IB comparison (Figure 9d); however, GOES-16 has analog to digital converter quantization problems that may mask arcjet noise. A detailed analysis of the arcjet contamination frequency content should be performed using improved measurements from GOES-17.

6. Conclusions

Arcjet thrusters on GOES-16 introduce an ~20 nT local magnetic disturbance that adversely impacts the operational and scientific utility of the magnetometer data. The magnetic disturbance has a repeatable linear relationship with the ambient magnetic field, allowing the data to be corrected during arcjet events. Correction parameters were derived using 63 arcjet events for GOES-16, and the residual errors in the corrected data are <1.5 nT. Startup transients and arcjet flag timing cause the correction to be invalid for the initial 5 min and the final 5 s of each arcjet event. Preliminary analysis suggests that the instrument noise is similar to the nominal performance during arcjet operations, although detailed frequency analysis of arcjet contaminated data has not been performed. The correction algorithm described here has recently been applied to GOES-16, and the data are available to the public.

Acknowledgments
The authors thank the GOES-R magnetometer teams at NASA GSFC and Lockheed Martin for their efforts in understanding and improving GOES-R magnetometer measurements, and the NOAA NCEI Space Weather Group for their work involving GOES-R ground processing and data stewardship. The data in this study can be accessed at https://data.ngdc.noaa.gov/platforms/solar-space-observing-satellites/goes/goes16/l2/data/magn-l2-hires/.

References

Bogorad, A., Likar, J., Deeter, M., August, K., Doorley, G., & Herschitz, R. (2008). Radiated emissions and magnetic field characterization of a 2-kW electrothermal propulsion system. *IEEE Transactions on Electromagnetic Compatibility*, *50*(3). https://doi.org/10.1109/TEMC.2008.927941

Califf, S., Loto'aniu, T. M., Early, D., & Grotenhuis, M. (2019). Arcjet thruster influence on local magnetic field measurements from a geostationary satellite. *Journal of Spacecraft and Rockets*. https://doi.org/10.2514/1.A34546

Cohen, R., Gerrard, A. J., Lanzerotti, L. J., Soto-Chavez, A. R., Kim, H., & Manweiler, J. W. (2017). Climatology of high-β plasma measurements in Earth's inner magnetosphere. *Journal of Geophysical Research: Space Physics*, *122*, 711–726. https://doi.org/10.1002/2016JA022513

Dichter, B., Galicia, G., McGarity, J., Tsui, S., Golightly, M., Lopate, C., & Connell, J. (2015). Specification, design, and calibration of the space weather suite of instruments on the NOAA GOES-R Program Spacecraft. *IEEE Transactions on Nuclear Science*, *62*(6).

Engebretson, M. J., Posch, J. L., Wygant, J. R., Kletzing, C. A., Lessard, M. R., Huang, C. L., et al. (2015). Van Allen probes, NOAA, GOES, and ground observations of an intense EMIC wave event extending over 12 h in magnetic local time. *Journal of Geophysical Research: Space Physics*, *120*, 5465–5488. https://doi.org/10.1002/2015JA021227

Iijima, T., Watanabe, M., Poterma, T. A., Zanetti, L. J., Kan, J. R., & Akasofu, S. I. (1993). Substorm currents in the equatorial magnetotail. *Journal of Geophysical Research*, *98*(A10), 17283–17298. https://doi.org/10.1029/93JA01644

Likar, J., Bogorad, A., Malko, T., Goodzeit, N., Galofaro, J., & Mandell, M. (2006). Interaction of charged spacecraft with electric propulsion plume: On orbit data and ground test results. *IEEE Transactions on Nuclear Science*, *53*(6), 3602–3606. https://doi.org/10.1109/TNS.2006.885107

Loto'aniu, T. M., Redmon, R., Califf, S., Singer, H. J., Rowland, W., Macintyre, S., et al. (2019). The GOES-16 spacecraft science magnetometer. *Space Science Reviews*, *215*, 32. https://doi.org/10.1007/s11214-019-0600-3

Nagai, T., Shinohara, I., Singer, H. J., Rodriguez, J., & Onsager, T. G. (2019). Proton and electron injection path at geosynchronous altitude. *Journal of Geophysical Research: Space Physics*, *124*, 4083–4103. https://doi.org/10.1029/2018JA026281

Pollard, J., Masuda, I., & Gotoh, Y. (2001). Plume mass spectrometry with a hydrazine arcjet thruster. *Journal of Spacecraft and Rockets*, *38*(3), 411–416.

Shprits, Y., Elkington, S., Meredith, N., & Subbotin, D. (2008). Review of modeling of losses and sources of relativistic electrons in the outer radiation belt I: Radial transport. *Journal of Atmospheric and Solar-Terrestrial Physics*, *70*, 1679–1693. https://doi.org/10.1016/j.jastp.2008.06.008

Shprits, Y., Subbotin, D., Meredith, N., & Elkington, S. (2008). Review of modeling of losses and sources of relativistic electrons in the outer radiation belt II: Local acceleration and loss. *Journal of Atmospheric and Solar-Terrestrial Physics*, *70*, 1694–1717. https://doi.org/10.1016/j.jastp.2008.06.014

Sibeck, D. G., Kudela, K., Lepping, R. P., Lin, R., Nemecek, Z., Nozdrachev, M. N., et al. (2000). Magnetopause motion driven by interplanetary magnetic field variations. *Journal of Geophysical Research*, *104*(A11), 25,155–25,169. https://doi.org/10.1029/2000JA900109

Singer, H. J., Hughes, W. J., Fougere, P. F., & Knecht, D. J. (1983). The localization of Pi 2 pulsations: Ground-satellite observations. *Journal of Geophysical Research*, *88*(A9), 7029–7036. https://doi.org/10.1029/JA088iA09p07029

Singer, H. J., Matheson, L., Grubb, R., Newman, A., & Bouwer, S. D. (1996). Monitoring space weather with the GOES magnetometers. In E. R. Washwell (Ed.), *GOES-8 and Beyond, Proc. SPIE, vol. 2812*, (pp. 299–308). Bellingham, Wash: Int. Soc. for Opt. Eng. https://doi.org/10.1117/12.254077

Takahashi, K., Glassmeier, K.-H., Angelopoulos, V., Bonnell, J., Nishimura, Y., Singer, H. J., & Russell, C. T. (2011). Multisatellite observations of a giant pulsation event. *Journal of Geophysical Research*, *116*, A11223. https://doi.org/10.1029/2011JA016955

Tsyganenko, N. A., & Sitnov, M. I. (2005). Modeling the dynamics of the inner magnetosphere during strong geomagnetic storms. *Journal of Geophysical Research*, *110*, A03208. https://doi.org/10.1029/2004JA010798